Tuning the Density Profile of Dendritic Polyelectrolytes

P. Welch and M. Muthukumar*

Polymer Science and Engineering Department, University of Massachusetts, Amherst, Massachusetts 01003

Received February 9, 1998; Revised Manuscript Received June 4, 1998

ABSTRACT: Using Monte Carlo simulations, we demonstrate that the shape of the intramolecular density profile of dendritic polyelectrolytes in solution can be tailored by varying the ionic strength of the solvent. Further, we find that a reversible transition between a "dense core" and a "dense shell" dendritic structure may be observed as the ionic strength is cycled from high to low. We present the necessary conditions in terms of salt concentration and various molecular variables such as generation number, spacer length, and number of charges, for realizing the potential of dendrimers as hosts in controlled-release and similar applications.

1. Introduction

The potential application of dendrimers in an array of technologically important roles has fueled the rapid growth of research in this field. A wide synthetic variety of dendrimers have been made with the aim of utilizing these molecules as hosts in controlled-release systems and as catalytic substrates.[1−3] The nature of the intramolecular density profile and the position of the terminal groups are critical in these applications. Ideally, the branches of the dendrimer would be highly extended at each generation of growth, with branch termini lying at the periphery of the molecule, as illustrated in Figure 1A. Several theoretical[4−12] and experimental[13−20] studies have addressed the possibility of this occurring in flexible dendritic systems. Some experimental evidence,[16−20] however, suggests that this behavior is not realized. Consideration of the conformational entropy of the molecule provides an understanding of the observed phenomena. To maximize the entropy, flexible dendrimers access many conformations that are inconsistent with the "dense shell" picture.[4] This exploration of phase space results in a "dense core"[5,7−12] average conformation, as pictured in Figure 1B. If, however, the extended branch conformations were made far more energetically favorable, then the entropy would be reduced to accommodate this energy difference, and the dense shell picture would be recovered. In this article we present a prescription for achieving this goal by exploiting Coulombic interactions.

In polyelectrolytic dendrimers, charge−charge repulsions may be minimized by forcing the charged moieties as far apart as possible. This should result in an expansion of the dendrimer with a corresponding rearrangement of the density profile. The DOSY NMR studies of Young and co-workers[21] and the SANS work of Briber and co-workers[22] both suggest this. These studies indicate that changing the pH of dendritic solutions results in a corresponding change in observed conformational properties. We explore this polyelectrolytic behavior in this study. Our results indicate not only that the dense shell picture may be realized, but also that the intramolecular density profile may be tuned from that of the dense core to that of the dense shell model with experimentally accessible parameters such as salt concentration or solvent pH, as illustrated in Figure 1.

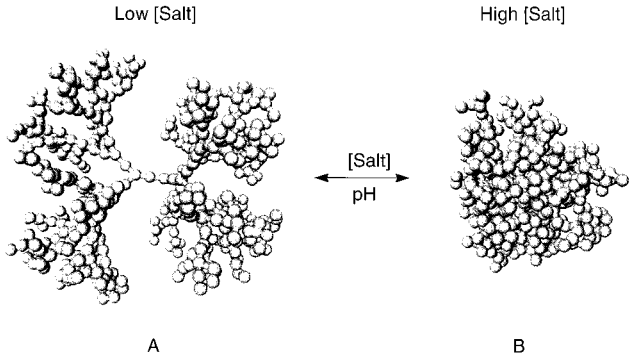

Figure 1. (A) Hollow core, "dense shell" picture. (B) "Dense core" picture. These are representative snapshots from the statistical ensembles generated in this study for the sixth generation with two springs between branch points.

To test this hypothesis, we applied the Monte Carlo computer simulation technique to the problem. The details of the model and algorithm are presented in section 2. In section 3, results that support our conjecture and a brief discussion of the possible applications of these findings are presented. A summary is provided in section 4.

2. Model and Simulation Technique

2.1. Model. A bead−spring, united atom model was utilized to represent the synthetic dendrimers, as shown in Figure 2. The springs play the role of bonds and the beads that of the molecule's mass. Each bead is of the same diameter. The coarse-grained models studied are topologically the analogue of poly(propylenimine) dendrimer. The unit charge was placed at all branch junctions and terminal groups, corresponding to a fully methylated or highly charged pH-sensitive synthetic system. The charged beads are illustrated in gray in Figure 2.

2.2. Energetics. Bonded interactions, excluded volume interactions, and charge−charge repulsions were considered in our study, as illustrated in Figure 2. The energetics of the model dendrimers were described by the following potential:

S0024-9297(98)00198-3 CCC: $15.00 © 1998 American Chemical Society
Published on Web 08/05/1998

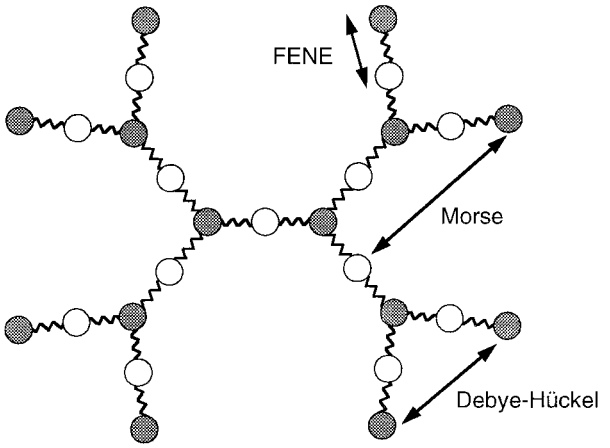

Figure 2. Bead−spring model employed in this study. The charged beads are gray.

$$\frac{U}{k_B T} = -KR^2 \sum_{i=1}^{N-1} \log\left[1 - \left(\frac{l_i - l_o}{R}\right)^2\right] + \frac{\sigma}{k_B T} \sum_{i,j=1}^{N} [(e^{-\alpha(r_{ij}-d)} - 1)^2 - 1] + l_B \sum_{i,j=1}^{N_f'} \frac{e^{-\kappa r_{ij}}}{r_{ij}} \quad (1)$$

The first term, a finitely extensible nonlinear elastic (FENE) potential, maintains the elastic connectivity of the bonds. This term permits fluctuations in the statistical bond length to facilitate equilibration of the model. The FENE is similar to the harmonic, "spring" potential but maintains a maximum and minimum limit on the bond length. Here, N is the total number of beads in the molecule and K is the spring constant. $R = l_{max} - l_o$ with $l_o = (l_{max} + l_{min})/2$. l_i, l_{max}, and l_{min} are the length of bond i, the maximum, and the minimum bond lengths, respectively. The values of the parameters were chosen to scale the simulation in units of Bjerrum length and to prevent the occurrence of phantom chains. The value of the Bjerrum length, l_B, in water at room temperature is 7.1 Å.[23] In synthetic systems, the distance between branch points is estimated to be on the order of 5 Å. For model systems with one spring between branch points, l_o should correspond to this experimental value. Therefore, we set $l_o = 5$ Å$/l_B = 0.7$ to yield one simulational unit equal to 7.1 Å. To prevent nonphysical bond crossing, after Binder et al.,[24] we have taken $K = 20.0$, $l_{min} = 0.4$, and $l_{max} = 1.0$.

The second term, the Morse potential, models the excluded volume interactions between nonbonded beads. Similar to the Lennard-Jones potential, this term is characterized by a repulsive core at short distances and an attractive tail at long distances. Therefore, simulations may be performed in good, Θ, and poor solvents. However, this potential is more computationally efficient because the attractive tail falls off more rapidly with distance than does the Lennard-Jones expression. Thus, a linked-cell technique was employed to truncate this term at a length of one cell box. σ and α are strength and range parameters, respectively. r_{ij} is the distance between beads i and j. d is the bead diameter. To ensure computational efficiency, after Binder et al.,[24] we chose $\alpha = 24.0$ such that the Morse term falls to zero for $r_{ij} \geq 1.25d$. Thus, $d = 0.8$ yields a linked-cell of unit dimension. σ was set to unity and solvent quality determined by k_BT, the thermal energy. Both the FENE and Morse potentials were hashed and results compared with nonhashed, exact simulations. No difference in accuracy was observed for the parameters chosen.

The third term, the Debye−Hückel potential, approximates the repulsive Coulombic interactions. This term allows for the parametrization of solvent ionic strength via κ, the inverse Debye screening length, which is proportional to the added salt concentration.

$$\kappa^2 = 4\pi l_B \sum_i c_i z_i^2 \quad (2)$$

Here, c_i and z_i are the concentration and valence of the ith ion, respectively. The potential falls off rapidly at low values of Debye length, corresponding to high salt concentrations but is long-ranged for large values, representing low salt concentrations. Σ' indicates that the summation runs over N_f trifunctional and terminal beads. κ^{-1} was adjusted within the range of experimentally obtainable values, 3−300 Å, corresponding to salt concentrations of 1 M to 0.1 mM. This term was calculated exactly for every pairwise interaction in the system: no truncation was performed on the charge−charge interactions.

Since our objective was to simulate polyelectrolytic dendrimers in good solvent conditions, solvent quality was studied for noncharged analogues by analysis of the dependence of the mean-squared radius of gyration, $\langle R_g^2 \rangle$ relative to its value at Θ-conditions, $\langle R_g^2 \rangle_\Theta$, as a function of temperature. $\langle R_g^2 \rangle_\Theta$ was determined from the Gaussian form factor via Guinier law plots. The details of these calculations are outlined in ref 25. k_BT was set to 0.7, well within the good solvent region for these models.

2.3. Algorithm. Metropolis Monte Carlo simulations employing a bond-fluctuation algorithm adopted from Milchev and Binder[24] were used to generate the statistical ensembles. Random self-avoiding walks complying with the bond length constraints were generated for initial conditions. These configurations were then relaxed for 30 000 perturbations prior to collecting statistics. The algorithm is straightforward. A bead is chosen at random and its location perturbed by ΔX, ΔY, and ΔZ in the range of ±0.5 simulational units. The energy change, ΔU, for the transition from the prior conformation to the new conformation is then calculated. If ΔU is negative, the new conformation is accepted. If not, it is accepted or rejected according to the Metropolis criteria.[26] Specifically, a random number in the range of 0 to 1 is chosen. If the random number is less than the Boltzmann factor for the transition, $e^{-\Delta U/k_B T}$, then the new conformation is accepted. Otherwise, the previous conformation is restored. This process is repeated for millions of cycles and the physical properties of the molecule are calculated every 10 000 Monte Carlo steps, each step representing N perturbations. These instantaneous values are used to generate running averages.

Three variables were examined in this study: the number of generations of growth, the number of springs and noncharged beads between branch points, and κ^{-1}. Statistics were collected for 3 to 6 million Monte Carlo steps. Approximately one-third of the perturbations were successful, leading to ensemble populations of at least 1 million configurations per simulation. Rapid equilibration of the models was observed. Doubling the number of Monte Carlo steps led to only a 0.7% change in $\langle R_g^2 \rangle$ for the largest model studied.

3. Results and Discussion

3.1. Scaling Analysis. Monte Carlo trajectories were constructed from $\langle R_g^2 \rangle$ to monitor the approach to equilibrium. A strong dependence of $\langle R_g^2 \rangle$ on κ and N was observed. An analysis of these results was facilitated by a simple Flory argument. The conformational free energy for polyelectrolytic dendrimers is governed by three components: an elastic connectivity term, an excluded volume term, and a Coulombic interaction term.

$$\frac{F}{k_B T} = F_{\text{elastic}} + F_{\text{excluded}} + F_{\text{Coulombic}} \tag{3}$$

$F_{elastic}$ should, as in the linear case, reflect the scaling behavior of dendrimers without excluded volume. Zimm and Stockmayer[27] showed that $R_g^2 \propto N^{1/2}$ for random dendritic molecules. Thus,

$$F_{\text{elastic}} \propto \frac{R_g^2}{N^{1/2}} \tag{4}$$

Examination of the pairwise interaction portion of the Edwards Hamiltonian yields the sought after dependence for the excluded volume and Coulombic repulsion terms. In the limit of high salt concentration, the two terms may be combined into an effective delta function potential.[28]

$$\frac{H}{k_B T} = \frac{1}{2l_0^2}\int_0^{Nl_0} \mathrm{d}s \int_0^{Nl_0} \mathrm{d}s' \delta[\vec{R}(s) - \vec{R}(s')]\left(w + \frac{4\pi l_B}{\kappa^2}\right) \tag{5}$$

Here, w is the familiar effective excluded volume interaction magnitude and is given by the binary-cluster integral:

$$w = \int \mathrm{d}^3 r_{ij} \, [1 - \mathrm{e}^{-u_{ij}/k_B T}] \tag{6}$$

u_{ij} is the pairwise nonbonded interaction, the Morse potential in this study. Numerical evaluation of eq 6 yields a value of 0.11 for w in this study. This was found to be in good agreement with the value obtained by fitting data from simulated linear molecules with the well-known Flory crossover equation.[29] $\vec{R}(s)$ is the spatial location of the segments. s is the contour position variable along the chain. The delta function contributes a R_g^{-3} scaling. Thus,

$$F_{\text{excluded}} + F_{\text{Coulombic}} \propto \left(w + \frac{4\pi l_B}{\kappa^2}\right)\frac{N^2}{R_g^3} \tag{7}$$

Combination of eqs 4 and 7 and minimization of $F/k_B T$ with respect to R_g yields the following expected scaling behavior for higher salt concentrations:

$$\frac{R_g}{N^{1/4}} \propto \left[\left(w + \frac{4\pi l_B}{\kappa^2}\right)N^{5/4}\right]^{1/5} \tag{8}$$

Figure 3 illustrates the simulations' agreement with this prediction for generations three, four, and five with one, two, and four springs between branch points. The predicted behavior is observed for much of the data. The scaling argument is most effective at reducing the data for high values of κ corresponding to the high salt concentration limit, and for four springs between branch points, corresponding to higher values of N where the mean-field nature of the treatment is expected to be

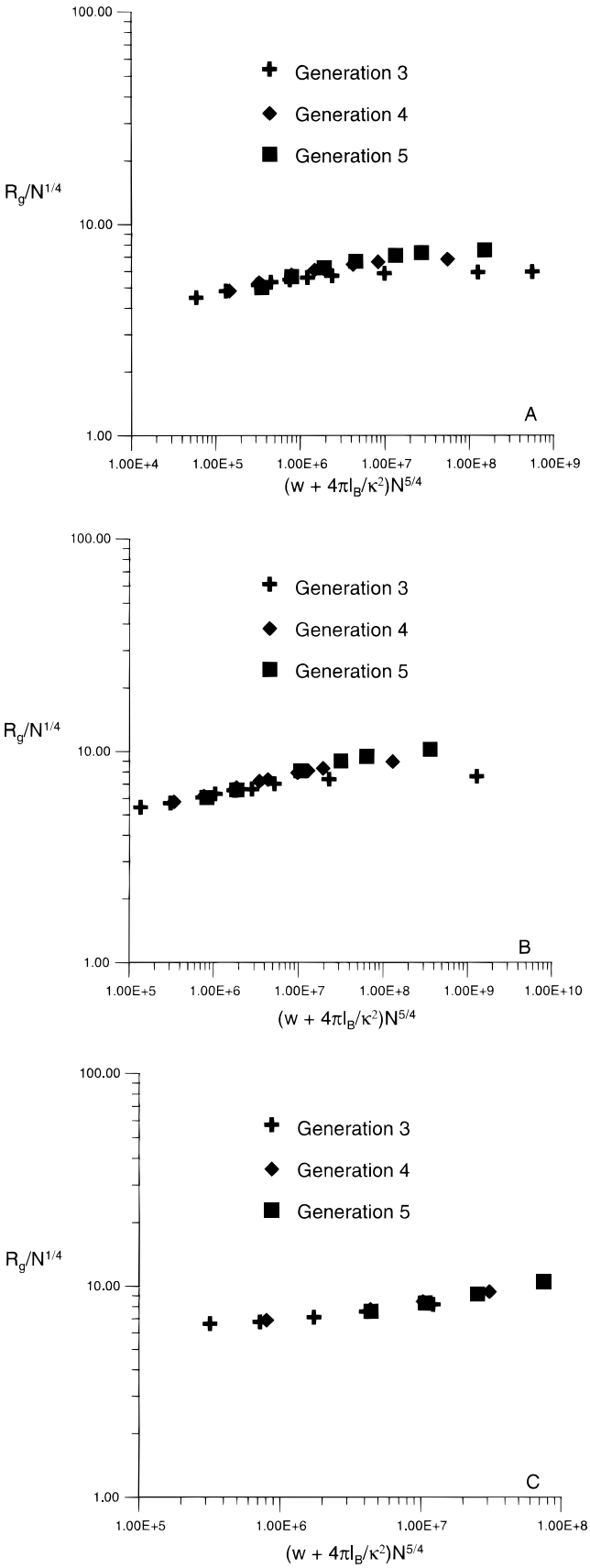

Figure 3. $\langle R_g^2 \rangle^{1/2}$ as a function of N and κ for the, third, fourth, and fifth generations. Data for one, two, and four springs between branch points are presented in (A)−(C), respectively. All lengths are in units of Angstroms.

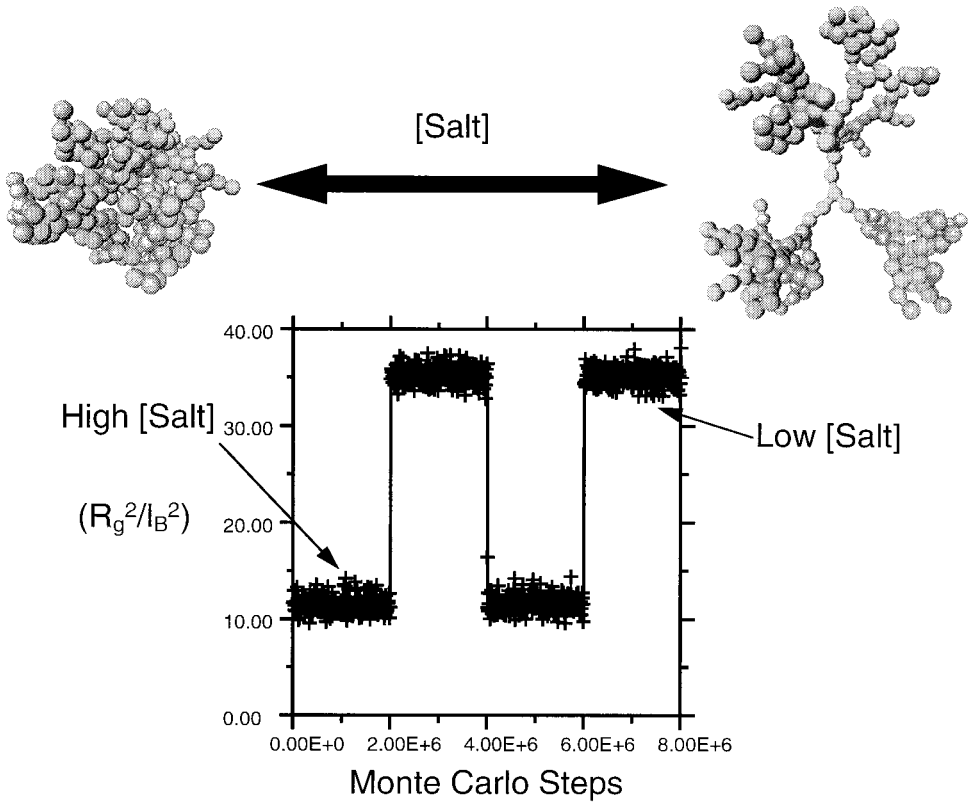

Figure 4. Smart behavior demonstrated in a polyelectrolytic fifth generation dendrimer with two springs between branch points. κ^{-1} was cycled from 3 Å (high salt concentration) to 300 Å (low salt concentration).

more applicable. However, the simulations included Debye lengths spanning the range from high to low salt concentrations. This is reflected in Figure 3 by the deviation away from the predicted behavior at low values of κ and by the slope of approximately $^1/_{10}$ as opposed to the predicted $^1/_5$.

3.2. Smart Behavior Observed. Figure 4 exemplifies the "smart" behavior predicted for these molecules. Results from a single simulation of a fifth generation dendrimer with two springs between branch points, in which κ^{-1} was cycled from 3 to 300 Å, are presented. This figure demonstrates not only that a large percent change in $\langle R_g^2 \rangle$, 65% in this case, is effected with varying Coulombic screening but also that the proposed corresponding conformational rearrangement is achieved: the model dendrimer redistributes its mass from a dense core picture to that reflecting a dense shell representation. This figure also demonstrates two important traits of the simulation. Since the same average value of $\langle R_g^2 \rangle$ is recovered rapidly from differing initial conformations, the results indicate the algorithm's ergodicity and speed of equilibration.

3.3. Density Profiles. The density profiles better illustrate the transition from a dense core to a dense shell average conformation. The average density profiles were calculated by dividing the space around the configurational center of the model dendrimers into concentric shells of thickness d. The average segment density in each shell at a distance r away from the center, $\langle \rho(r) \rangle$ is given as:

$$\langle \rho(r) \rangle = \langle n(r) \rangle \frac{V_b}{V_s(r)} \tag{9}$$

$\langle n(r) \rangle$ is the ensemble average number of beads in the shell at distance r. V_b and $V_s(r)$ are the volumes of the beads and shells, respectively.

At $\kappa^{-1} = 3$ Å, corresponding to a high salt concentration, the density is observed to be monotonically decaying with radial distance in accordance with the dense core picture, as predicted by Lescanec and Muthukumar.[5] However, as κ^{-1} is increased to 64 Å, corresponding to low salt concentration, a minimum occurs near the core, indicating increased porosity in the interior of the molecule. This minimum is followed by a secondary peak in density near the model's periphery, approaching the dense shell picture. The depth of this minimum and the radial position of the secondary peak increases with increasing κ^{-1}. This effect is most pronounced for the higher generations and is absent in generations one and two for one, two, and four springs between branch points. Figure 5 is representative of the density profile behavior. Results for the fifth generation of growth with two springs between branch points are illustrated. The density profiles of the terminal segments were also examined. Regardless of the value of κ^{-1}, the terminal groups are found to be dispersed throughout the molecule. However, the location of maximum terminal group density does shift toward the periphery with increasing κ^{-1}. This behavior is demonstrated in Figure 6, in which results for the fifth generation dendrimer with four springs between branch points are illustrated. κ^{-1} was cycled from 3 to 300 Å. In the high salt limit the maximum terminal group density lies below the $\langle R_g^2 \rangle^{1/2}/l_B$ value of 4.80. However, in the low salt limit the maximum falls above the $\langle R_g^2 \rangle^{1/2}/l_B$ value of 9.22. Further, the value of $\langle R_g^2 \rangle_T$ of the terminal groups is found to be higher than that for the whole molecule, regardless of the value of κ^{-1} and the corresponding terminal group distribution. For example, in simula-

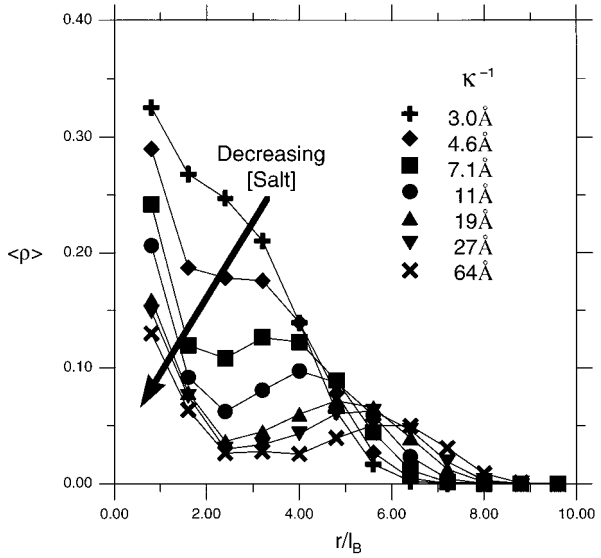

Figure 5. Typical density profiles. Data for a fifth generation dendrimer with two springs between branch points are shown.

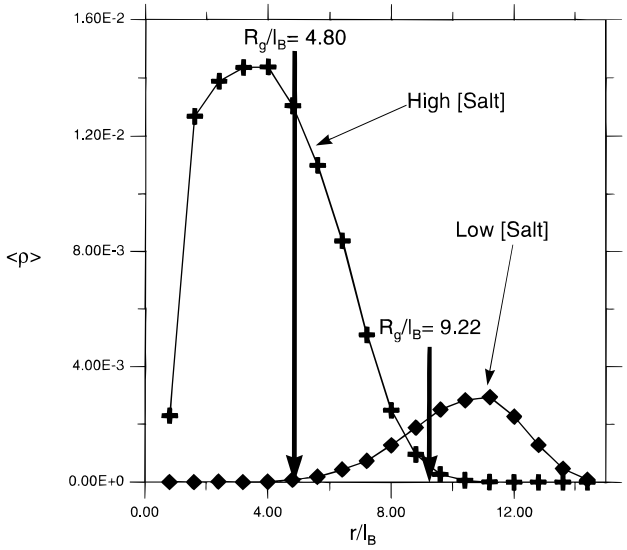

Figure 6. Typical density profiles for the terminal segments. Data for a fifth generation dendrimer with four springs between branch points are shown.

tions of sixth generation monocentric model dendrimers analogous to poly(amido amine) with an ammonia core and charged terminal groups, the ratio of $\langle R_g^2\rangle_T/\langle R_g^2\rangle$ shifts from 1.81 to 4.65 when κ^{-1} is varied from 3 to 300 Å.

3.4. Form Factors. To facilitate comparison with SANS data, the spherically averaged single particle form factor, $S(\vec{q})$, was calculated.

$$S(\vec{q}) = \frac{1}{N^2}\sum_{i=1}^{N}\sum_{j=1}^{N}\frac{\sin(\vec{q}\cdot r_{\bar{i}j})}{\vec{q}\cdot r_{\bar{i}j}} \tag{10}$$

where

$$|\vec{q}| = \frac{4\pi}{\lambda}\sin\left(\frac{\theta}{2}\right) \tag{11}$$

A secondary peak in the single particle form factor is observed to arise, and the magnitude of the peak is seen to increase with increasing κ^{-1} for generations three and

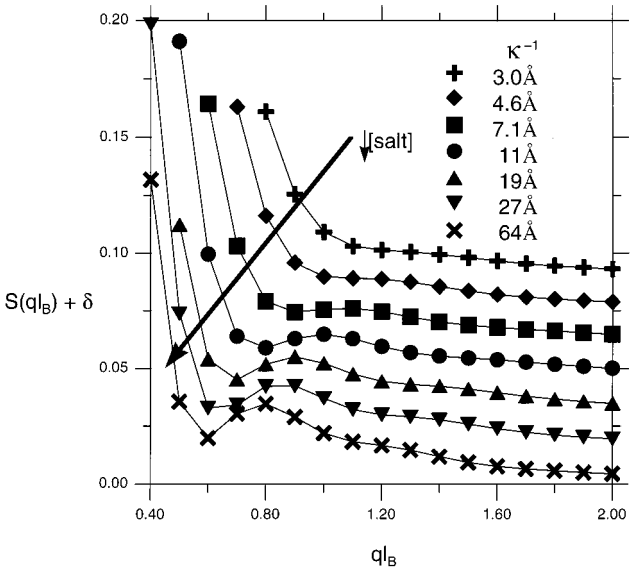

Figure 7. Typical structure factors for the model dendrimers. The data have been shifted along the *y*-axis by $\delta = n0.015$ with $n = 0$ for $\kappa^{-1} = 64$ Å and $n = 6$ for $\kappa^{-1} = 3$ Å. Data for a fifth generation dendrimer with two springs between branch points are shown.

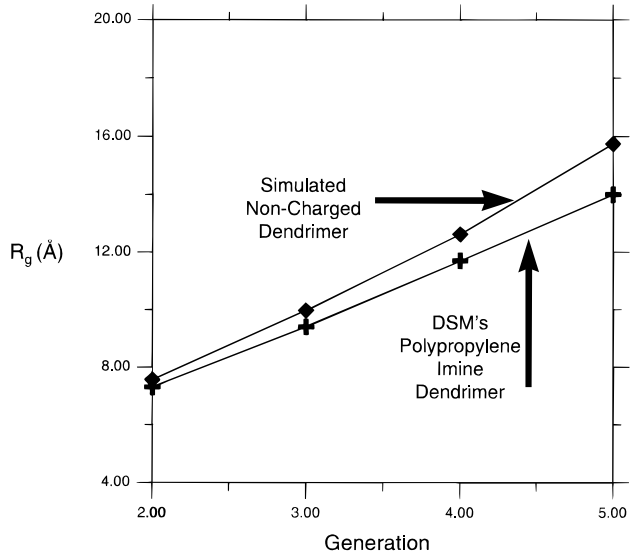

Figure 8. Comparison of experimental results for poly(propylenimine) dendrimers and the Monte Carlo results for their bead−spring, topological analogues in the noncharged limit.

above. The location of the maximum shifts to lower values of $|\vec{q}|$ with increasing κ^{-1}. This peak corresponds to the development of internal order whose length scale increases with decreasing Coulombic screening. This behavior, shown in Figure 7, is in qualitative agreement with experimental observations for poly(amido amine) dendrimers studied via SANS,[22] though the experiments were carried out at a higher concentration and include intermolecular correlations. Results for the fifth generation of growth with four springs between branch points are presented with κ^{-1} in the range of 3 to 64 Å.

3.5. Noncharged Limit. Figure 8 illustrates the model's relevance to experimentally realizable synthetic systems. SANS results for poly(propylenimine) dendrimers from the literature[30] and our simulation results in the noncharged limit are presented. Good agreement is observed with a slight overprediction at higher

generations. This systematic deviation likely arises from the thermodynamic nature of the simulation. Specifically, the exact value of k_BT in the simulational units corresponding to the solvent quality or magnitude of the excluded volume interaction of the experimental system is difficult to ascertain. Nonetheless, this comparison does illustrate the applicability of the model and algorithm to the study of synthetic systems.

3.6. Discussion. These results demonstrate two technologically important properties of polyelectrolytic dendrimers. First, the position of most terminal moieties in the low electrostatic screening limit is on the surface of the molecule. This is of particular significance for the proposed catalytic and high-density cross-linking applications that would take advantage of the large number of reactive terminal groups. Second, not only may the hollow core conformation be obtained in the limit of low salt concentration or by adjusting the pH, but the density profile may also be tuned to the dense core picture by simply adjusting external experimental constraints. This behavior is requisite for the controlled release applications proposed for these molecules.[1−3] One might imagine trapping a small molecule inside a polyelectrolytic dendrimer at low salt concentration or at low pH. Then, the small molecule, a drug for example, may be delivered by placing the guest−host complex in a high salt or neutral pH medium to affect a rearrangement of the density profile. This rearrangement may be expected to eject the guest from its dendritic cage.

4. Conclusions

In conclusion, the dilute solution behavior of polyelectrolytic dendrimers in solvents of various ionic strengths has been examined by Monte Carlo simulations. The intramolecular density profile is observed to be heavily dependent upon the Debye screening length. On the basis of these results, we predict that the density profiles of synthetic systems are tunable from that of the dense core to that of the dense shell picture by manipulation of the salt concentration or pH in aqueous solutions. Studies in the literature suggest this possibility, but we present here the first clear demonstration of the large changes in molecular dimension that are realizable. Finally, qualitative agreement with scattering experiments on pH sensitive dendrimers is observed.

Acknowledgment is made to NSF Grant No. DMR 9625485. The authors are also grateful to Robert Lescanec for many fruitful conversations and guidance regarding the problem addressed here.

References and Notes

(1) Frechet, J. M. J. *Science* **1994**, *263*, 1710.
(2) Jansen, J. F. G. A.; de Brabander-van den Berg, E. M. M.; Meijer, E. W. *Science* **1994**, *266*, 1226.
(3) Jansen, J. F. G. A.; Meijer, E. W.; de Brabander-van den Berg, E. M. M. *Macromol. Symp.* **1996**, *102*, 27.
(4) de Gennes, P.-G.; Hervet, H. *J. Phys. Lett.* **1983**, *44*, L351.
(5) Lescanec, R. L.; Muthukumar, M. *Macromolecules* **1990**, *23*, 2280.
(6) Naylor, A.; Goddard, W.; Kiefer, G.; Tomalia, D. *J. Am. Chem. Soc.* **1989**, *111*, 2339.
(7) Mansfield, M.; Klushin, L. *Macromolecules* **1993**, *26*, 4262.
(8) Murat, M.; Grest, G. *Macromolecules* **1996**, *29*, 178.
(9) Mansfield, M. *Polymer* **1994**, *35*, 1827.
(10) Boris, D.; Rubinstein, M. *Macromolecules* **1996**, *29*, 7251.
(11) Chen, Z.; Cui, S. *J. Macromolecules* **1996**, *29*, 7943.
(12) Lue, L.; Prausnitz, J. *Macromolecules* **1997**, *30*, 6650.
(13) Bauer, B. J.; Topp, A.; Prosa, T. J.; Amis, E. J.; Yin, R.; Qin, D.; Tomalia, D. A. *Polym. Mater. Sci. Eng.* **1997**, *77*, 87.
(14) Amis, E. J.; Topp, A.; Bauer, B. J.; Tomalia, D. A. *Polym. Mater. Sci. Eng.* **1997**, *77*, 183.
(15) Valachovic, D. E.; Bauer, B. J.; Amis, E. J.; Tomalia, D. A. *Polym. Mater. Sci. Eng.* **1997**, *77*, 230.
(16) Meltzer, A.; Tirrell, D.; Jones, A.; Inglefield, P.; Hedstrand, D.; Tomalia, D. *Macromolecules* **1992**, *25*, 4541.
(17) Mansfield, M.; Klushin, L. *J. Phys. Chem.* **1992**, *96*, 3994.
(18) Mourey, T. H.; Turner, S. R.; Rubinstein, M.; Frechet, J. J.; Hawker, C. J.; Wooley, K. L. *Macromolecules* **1992**, *25*, 2401.
(19) Wooley, K. L.; Klug, C. A.; Tasaki, K.; Schaefer, J. *J. Am. Chem. Soc.* **1997**, *119*, 53.
(20) Gorman, C. B.; Hager, M. W.; Parkhurst, B. L.; Smith, J. C. *Macromolecules* **1998**, *31*, 815.
(21) Young, J. K.; Baker, G. R.; Newkome, G. R.; Morris, K. F.; Johnson, C. S. *Macromolecules* **1994**, *27*, 3464.
(22) Briber, R.; Bauer, B.; Hammouda, B.; Tomalia, D. *Polym. Mater. Sci. Eng.* **1992**, *67*, 430.
(23) Hara, M. *Polyelectrolytes*; Marcel Dekker: New York, 1993.
(24) Milchev, A.; Binder, K. *Macromol. Theory Simul.* **1994**, *3*, 915.
(25) Welch; P. M.; Mathias, L. J.; Lescanec, R. L. *Polym. Prepr.* **1996**, *37*, 250.
(26) Metropolis, N.; Rosenbluth, A. W.; Rosenbluth, M. N.; Teller, A. H.; Teller, E. J. *J. Chem. Phys.* **1953**, *21*, 1098.
(27) Zimm, B.; Stockmayer, W. *J. Chem. Phys.* **1949**, *17*, 1301.
(28) Muthukumar, M. *J. Chem. Phys.* **1987**, *86*, 7230.
(29) Yamakawa, H. *Modern Theory of Polymer Solutions*; Harper and Row: New York, 1971.
(30) de Brabander, E. M. M.; Brackman, J.; Mure-Mak, M.; de Man, H.; Hogeweg, M.; Keulen, J.; Scherrenberg, R.; Coussens, B.; Mengerink, Y.; van der Wal, S. *Macromol. Symp.* **1996**, *102*, 9.

MA980198W